Preliminary analysis of the flow field in a transparent model of a SRF cavity by PIV

Preliminary analysis of the flow field in a transparent model of a SRF cavity by PIV

F Cozzi[1,3], **G Pianello**[1], **A D'Ambros**[2], **C Pagani**[2], **D Sertore**[2]

[1] Politecnico Milano, Dipartimento di Energia, Via Lambruschini 4, Milano, Italy
[2] Istituto Nazionale di Fisica Nucleare-LASA, Via Fratelli Cervi 201, Segrate, Italy
[3] corresponding author: fabio.cozzi@polimi.it

Abstract. Niobium superconductive radio frequency cavities (SRF cavities) are commonly employed in linear accelerator; very pure, clean, and smooth internal walls are required to make the cavity working properly and with a high Q factor. Typically, to achieve a suitable surface quality the SRF cavities are subjected to a surface treatment called Buffered Chemical Polish (BCP), the latter uses a strong concentrated acids mixture flowing through the cavity to chemically etch a thin niobium layer (~250 μm). A viable way to understand and optimize the BCP process is by using computational fluid dynamic (CFD); however, the experimental validation of the numerical and physical models is required to confidently use CFD results. The aim of our work is to investigate the fluid dynamics of the BCP process by using the Particle Image Velocimetry (PIV) and the refractive index matching (RIM) techniques, and to provide data to validate CFD simulations. The paper describes and briefly analyse the experimental setup and the preliminary results achieved so far.

1. Introduction

Particle accelerators are among the most versatile instruments designed by physicists and built to produce high speed and high energy charged particles beams. Particle accelerators have been firstly conceived and developed to investigate the nature of matter and its fundamental governing laws. Today they have a vast number of applications in many technical and industrial fields unrelated to fundamental research. It has been estimated that there are approximately 30,000 accelerators worldwide. Of these, only about 1% are research machines with energies above 1 GeV, while about 44% are for radiotherapy, 41% for ion implantation, 9% for industrial processing and research, and 4% for biomedical and other low-energy research [1].

The PIP-II particle accelerator will be the new heart of Fermilab, featuring a brand-new, 800-MeV, leading-edge superconducting linear accelerator. INFN contributes to this project with the low beta section of the linear accelerator: the 36 superconductive cavities of this section, designed by INFN-LASA, will be produced and surface treated in industry and qualified through vertical cold test.

Superconductive cavities are complex and expensive device, built in niobium, that need a lot of care during production to ensure their design characteristics. Their purpose is to produce the intense electric fields thanks to which a charged particle can be accelerated. To ensure the high performance required by the project, after mechanical fabrication, it is necessary to treat the internal cavity surface to remove a layer of about 200 μm. The reason is that the superconducting RF current flows in a surface layer of about 40 nm deep, so every contamination and niobium crystal damage must be removed to assure good superconducting properties of that surface layer.

Two main polishing processes has been developed during years: buffered chemical polishing (BCP) and electro polishing (EP). Even if the overall behavior of these processes has been widely understood, there are still particular features that remains obscure. Some researchers have

demonstrated with experiments that asymmetry in wall removal rates is imputable to the fluid velocity, and etching rate at different fluid velocity can be fitted with a power law [2, 3, 4].

A viable way to better understand these processes is by using computational fluid dynamic (CFD), however, given the dangerousness of the acids, it is very difficult to create and validate a numerical model to describe their chemical and physical properties. Moreover, the uncertainties in the solution of fluid simulations are further increased by the complex geometry of a SRF cavity; thus, without an experimental validation, results from this type of simulations cannot be confidently used to improve the process. To this aim, a cooperation started between INFN-LASA and the Laboratory of Combustion and Optical Diagnostics (Politecnico di Milano) to experimentally investigate the fluid dynamics of the BCP process by means of the Particle Image Velocimetry (PIV) and the refractive index matching (RIM) technique. Even if PIP-II cavities will be treated with electro polishing, we chose the latter as baseline geometry and BCP as process to be analyze. We made this choice since the realization of a PIV experimental setup based on electro polishing is extremely complex in hydraulic and optical terms. BCP instead, is simpler and easier to realize. Being the acids mixture very toxic and dangerous it cannot be used in laboratory measurements, so a model fluid, a glycerol/water mixture, and a transparent model of the cavity are used. It must be noticed that our experimental set-up is not designed to faithfully replicate all the phenomena occurring during the PCB treatment, but only to faithfully replicate the fluid dynamic aspects of the process by exploiting the geometrical and dynamic similarity. While flow visualizations have been already reported in [2, 3], to the author's knowledge it is the first time that PIV and RIM techniques are applied to study the PCB treatment.

The aim of the paper is to report the experimental setup and the preliminary results achieved so far, it also shows the capability of the PIV and RIM techniques to provide potentially useful data to better understand and to improve the BCP process.

2. Experimental set-up and Techniques

2.1. The Refractive Index Matching technique

One of the most relevant issues regarding PIV and others optical measurements methods is the refraction of the light at the interfaces (solid-gas or solid-liquid), this leads to distortions or multiple images and hinder the use of any optical technique. The refractive index matching (RIM) technique consists in using a fluid and a transparent solid model having the same refractive index, by this way the refractive index field is spatially homogeneous and no optical distortion arose [5]. The transparent model is commonly called phantom, because when it is plunged into the matching fluid the fluid-solid interfaces are no more visible, and the model disappears from the view. Organic liquids, liquid mixtures or aqueous solutions can be used as matching fluid for different solid materials [4,5, 6]. The use of liquid mixture of two or more components allows to adjust the refractive index simply by changing the mass fractions of the components.

In our work, the PIV and the RIM techniques are adopted to analyze the flow field inside a transparent scaled version of the PIP-II low beta cavity. The cavity model is made of Sylgard 184, while the matching fluid is a mixture of water and glycerol (about 61% glycerol and 39 % water by mass). Sylgard 184 has a relatively low refractive index (about 1.41) and it allows the use of cheap, non-corrosive, non-toxic, water/glycerol mixtures as a RIM fluid [6, 7, 8].

The mixing and curing on Sylgard 184 affect the refractive index of the cured rubber [8], thus the composition of the matching water/glycerol mixture needs to be calibrated on the actual model. An Abbe refractometer is used to measure the RI of the silicone rubber and of several water/glycerol mixtures (at a wavelength of 589 nm, the Sodium D1-line). At a temperature of 24 °C, the measured RI of a cured sample of Sylgard 184, made from the same batch used to cast the model, is n_S=1.4118, and the matching fluid results to be a mixture of 60% glycerol and 40% water by weight, see Figure 1. The Helmers et al.'s polynomial fit [10] for water/glycerol mixtures is also reported in the same figure for comparison. The small systematic difference (less than 0.1%) between our results and the Helmers's fit could be ascribed to small differences in the actual compositions.

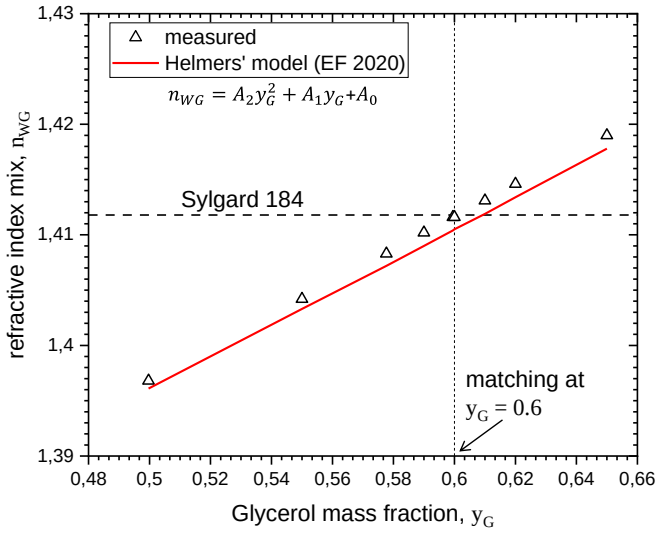

Figure 1. Measured refractive index of liquid mixtures (empty symbols), cured Sylgard 184 (horizontal dashed line) and polynomial fit for water/glycerol mixture from Helmers et al. [10] (solid red line). All data at 589 nm

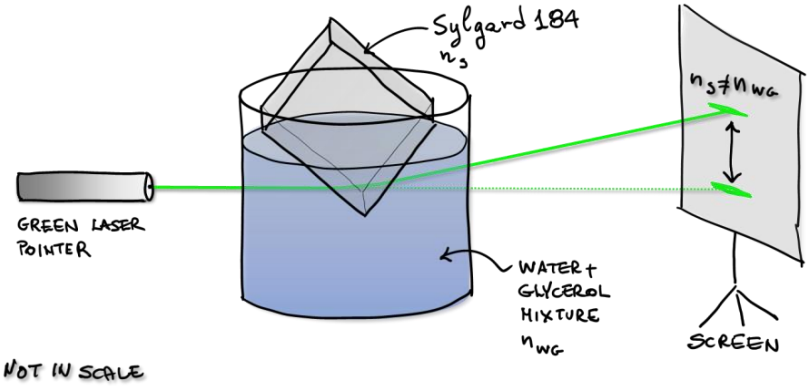

Figure 2. Technique to perform refractive index tuning. Laser beam path without the Sylgard sample (thin line). Refracted beam for mismatched solid and liquid samples (thick line).

To achieve a precise RI match, the mixture composition must be tuned at the wavelength of the PIV Laser (532 nm) which differs from that used in the Abbe refractometer. Several approaches are possible [5], and we implemented a simple method based on light refraction. A green laser pointer (532 nm wavelength) is shot through a Becker full of the liquid mixture to be tested, a screen is place far away from the laser (in our case ~10 m) and the position of the laser beam on the screen is recorded; then a prismatic sample (made from the same batch used for the phantom) is partially plunged in the liquid so to intercept the laser beam. Any mismatch between the solid and the liquid sample shows up by the deflection of the laser beam due to the refraction at the interfaces, Figure 2, the mixture composition is changed until the RI matching is achieved, and no beam deflection can be noticed. This procedure easily discriminates which of the two components is in excess, if the beam is deflected upwards the refractive index of the mixture, n_{GW}, is smaller than that of the silicone rubber, n_s, and more glycerol is needed, and vice versa for the other way round. In our case we start with the nominal composition (60% by weight of glycerol), and we slowly add glycerol until we got the RI match at a glycerol mass fraction of y_g=60.84%.

2.1.1. Fluid-dynamic and geometric similarity. Both the geometric and the fluid dynamic similarity are imposed to ensure the flow similarity between the model and the real flow, i.e., the Reynolds numbers must be the same, and the model must be a scaled replica of the real cavity. The Reynolds number, *Re*, is defined using the volumetric flow rate, Q, the area of a reference section, A, a reference length, L, and the kinematic viscosity of the fluid, ν, equation (1):

$$Re = \frac{QL}{A\nu} \tag{1}$$

the flow rate required by the dynamic similarity is given by equation (2), the latter obtained by combining equation (1) and the geometrical scale factor $M = L_{model}/L_{actual} = (A_{model}/A_{actual})^{1/2}$.

$$Q_{model} = Q_{actual} M \frac{\nu_{model}}{\nu_{actual}} \quad (2)$$

The model scale factor is $M = 1/4$, thus according to equation (2) and to data in Table 2, the water/glycerol flow rate required by the similarity is Q_{model} =2.5 l/min. The Reynolds number based on the injector diameter (8 mm) and the injection bulk velocity (0.82 m/s) is Re≅584, Table 1.

Table 1. Geometrical parameters and fluid properties of the real cavity and its model.

	Units	**Actual Cavity**	**Silicone Model**
fluid	% by mass	25 %, HF (40% in water) 25 %, HNO_3(65% in water) 50 %, H_3PO_4(85% in water)	glycerol 60.84% water 30.16%
D_{inlet}	m	0.032	0.008
density	kg/m^3	1490	1154
dynamic viscosity[a], μ	Pa·s	0.022 (at 15 °C)	0.013 (at 17 °C)
volumetric flow rate	l/min	13.5	2.5
Injection velocity	m/s	0.28	0.82
Reynolds number		584	584

[a] The dynamic viscosity of the water-glycerol mixture is evaluated according to Cheng at al. [11]

2.2. The Phantom Cavity, the aquarium, and the hydraulic plant.

The model is made by two symmetrical silicone blocks joined together to have an octagonal section, the two blocks are made by using a steel mold mirror polished, Figure 3. The internal empty space of the model replicates in a 1:4 scale the PIP-II low beta cavity shape and consists of five cells linked by irises and inlet and outlet channels. The model is about 0.3 m in height, while the inlet and outlet cylindrical channels have both a diameter of about 0.03 cm, Figure 4.

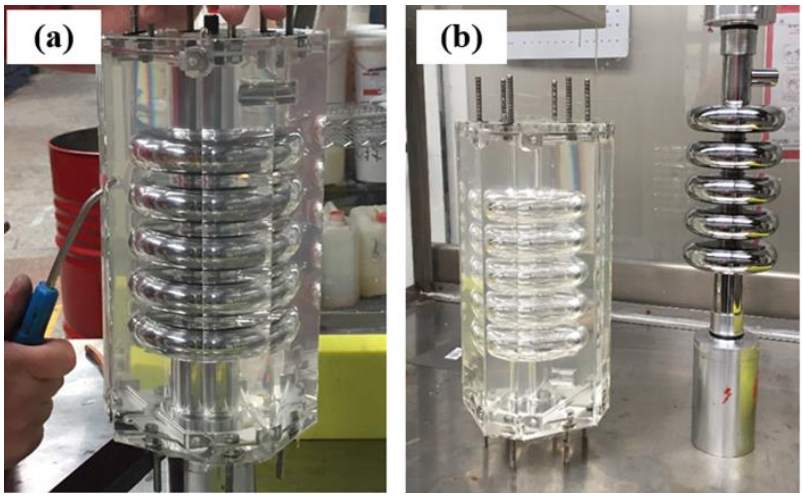

Figure 3. a) Separation of the two part of the model from the mold. b) The assembled model (left), and the stainless steel mold (right).

The model is placed inside a glass box, the aquarium, having an octagonal cross section, this allows to implement a stereo PIV configuration with 90° angular separation between the camera, with each PIV camera placed at 90° respect to the transparent wall; this eliminates aberrations arising in imaging performed through a thick transparent medium [12]. The aquarium is filled with the water/glycerol mixture and the model is almost invisible when submerged inside it. A photo of the empty aquarium with the model in place is shown in Figure 5.

To simulate the actual flow occurring during the BCP process the cavity model is inserted in the hydraulic plant shown in Figure 6. The tank A at height Z_A is filled with the water/glycerol mixture,

while the phantom and the collecting tank are located at a lower height Z_B. The fluid flow is achieved thanks to gravity only, and the height difference Z_A-Z_B is set so to compensate the circuit losses, the needle valve V_2 and the variable area flowmeter allow to control the flow rate. The RIM fluid is injected into the phantom from the bottom, through a hole of 8 mm in diameter, and it flows out from the top, Figure 5, then it is pumped back to tank A by a volumetric pump, Figure 6. By adjusting the pump flow rate, a steady flow is achieved.

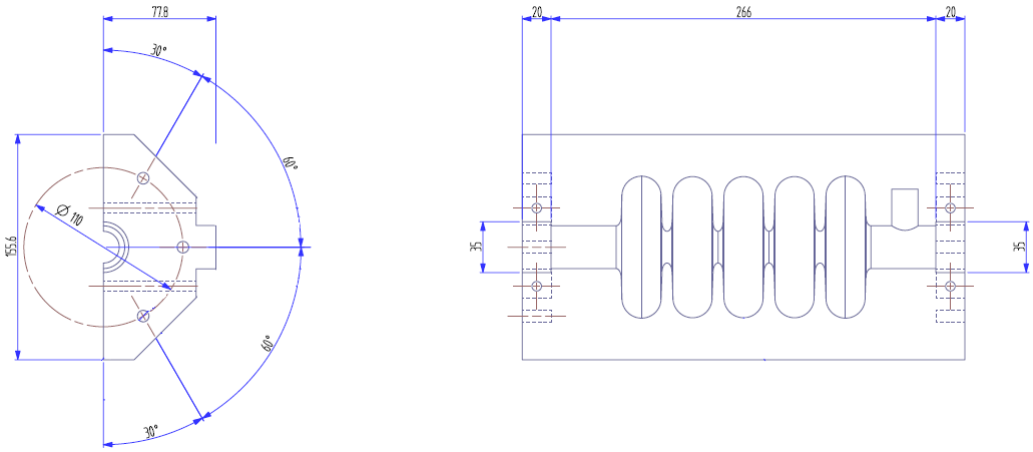

Figure 4. CAD drawing of half of cavity model.

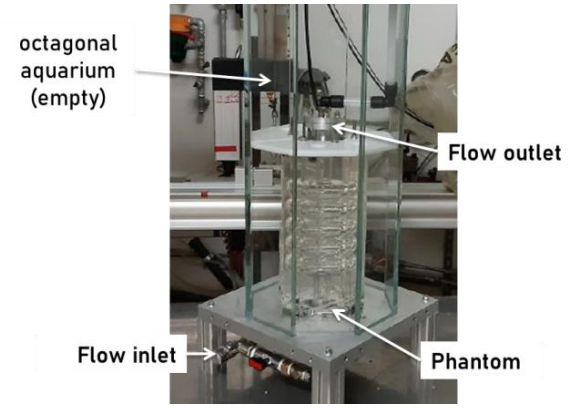

Figure 5. The SRF cavity model placed in the empty aquarium.

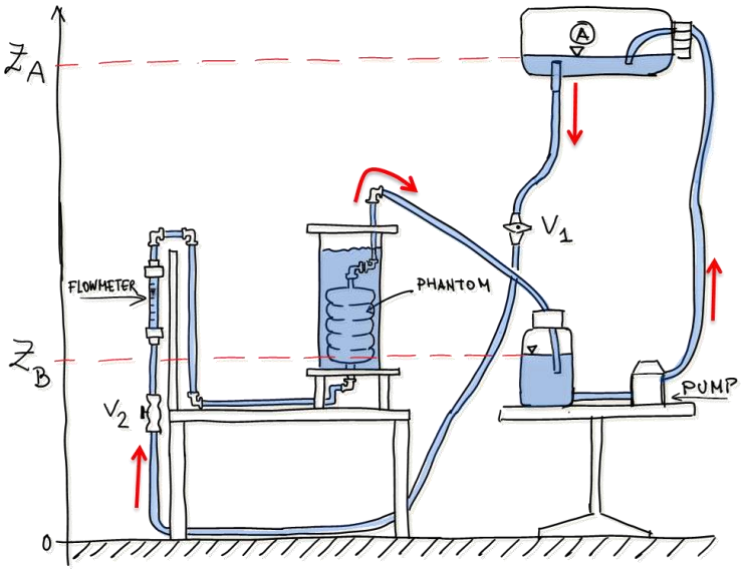

Figure 6. Sketch of the hydraulic plant

2.3. PIV system and measurements.

The experimental bench was realized and set-up at Laboratory of Combustion and Optical Diagnostics of Politecnico di Milano, and all tests were performed at an ambient temperature of about 17 °C. In this preliminary work, only one camera of the Stereo-PIV system was operative, thus we implemented a skewed but standard PIV, stereo-PIV measurements are planned in future experiments. The PIV system consisted of a double-pulsed Nd:YAG laser operating at λ = 532 nm with a maximum pulse energy of 200 mJ/pulse. The CCD camera has a resolution of 1344 * 1024 pixels, and it is equipped with a 60 mm focal length Micro-Nikkor lenses. Lens aperture is set to F#=11 and an interferential band-pass filter centered at 532 nm block ambient light. The seeding particles are glass hollow spheres of 9-13 μm in diameter, their density is about ρ_p= 1.1 g/cm^3, thus they are almost neutrally buoyant in the fluid mixture. Assuming the flow velocity and mixture properties reported in Table 2, the particles Stokes number is less than 0.001.

The CCD camera is mounted on a traversing system at an angle of 45° respect to the forward scattering direction of the laser sheet. The traversing system allows to move the camera with a resolution of 0.1 mm. The laser sheet is about 1 mm thick and is aligned with the axis of the phantom model. Three different fields of view are considered, they are of the same size but displaced each other of about 60 mm in the vertical direction. Double images with an inter frame time between 2.5 and 4 ms are acquired at a rate of 4 Hz, for each field of view 500 couples of images are acquired.

Image acquisition and analysis are performed with Dynamic Studio 7.1 software from Dantec Dynamics. Camera calibration is performed using a pinhole camera model including both radial and tangential distortions, the calibration target is a double side target dipped in the RIM fluid.

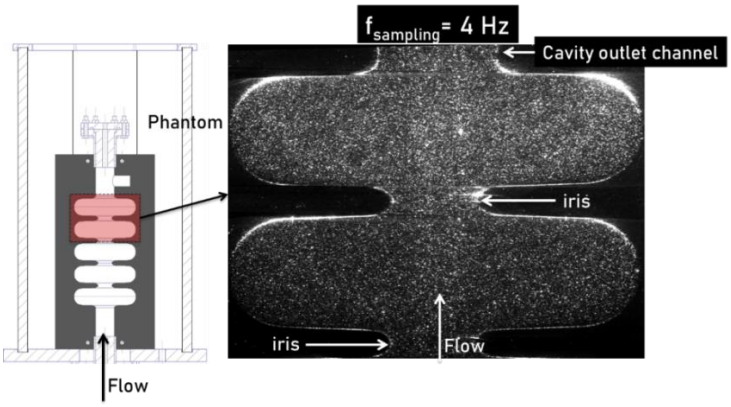

Figure 7. Example of a dewarped PIV image. The red rectangular region highlighted in the drawing to the left shows the location of the field of view.

Being acquired in skewed direction respect to the laser sheet, the PIV images are dewarped before being analyzed, Figure 7. A black mask applied to the dewarped images black out the solid region of the model and to some extent the annoying wall reflections. The correlation averaging method [13] is implemented to increases the signal to noise ratio and to allow the use of smaller interrogation windows, vector range validation is implemented to discard spurious vectors. The interrogation area (IA) is set to 16x16 pixels, with a 50% overlap, and the resulting vector spacing is about 0.75 × 0.75 mm^2.

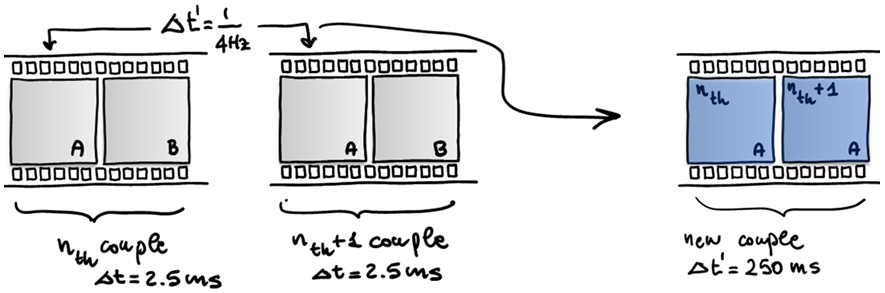

Figure 8. Procedure to generate double images with an inter frame time of 250 ms

To improve velocity resolution in the low velocity regions, i.e., those inside the lobes of each cell, a new set of 499 couples of images is built. This is done by pairing the first image of each of the 500 couples acquired at a frequency of 4 Hz, see Figure 8. This new set of double images is analyzed using the same method applied to the original ones, except a peak validation is enforce instead of the range validation. The inter frame time of the new dataset is $\Delta t = 1/4\ Hz^{-1}$= 250 ms, being 100 times longer than the original one the low velocities are accurately resolved, conversely the higher velocities are lost. To overcome such drawback a hybrid velocity map is generated, the mean velocity vectors belonging to the original map and having a module < 1 pixels are substituted by their corresponding vectors computed from the new dataset. The resulting hybrid velocity map is shown in Figure 10(a).

3. Experimental results

3.1. Flow field visualization

A preliminary analysis of the mean flow field structure is carried out by averaging together the first images of each of the 500 dewarped PIV images couples. Despite the seeding has been homogeneously dispersed and mixed with the RIM fluid, the resulting mean images evidence some inhomogeneities. At the beginning of each test the fluid inside the cavity is almost clean from seeding and it mixes with the seeded fluid as the fluid flows in the system. The PIV acquisition starts only when the images evidence a homogeneous seeding density. Nevertheless, the long fluid residence times inside the cells, and the slow laminar mixing between the central flow and the cells, hinder the achievement of perfectly homogeneous seeding condition. That inhomogeneity allows the flow field structure to appear in the mean image, and by stitching together the mean images the full flow field is revealed, Figure 9.

Figure 9 evidence an almost axisymmetric structure with a central jet flow (directed upward) originated by the fluid injection; due to the entrainment process the jet diameter grows moving downstream up to cell 4, further downstream its diameter stay approximately constraint by the aperture of irises. We suspect that a slight misalignment occurred between the laser sheet and the cavity axis for the PIV images containing cell 5 and the inlet region, thus the evolution of the central jet diameter in that region will have to be verified in future experiments.

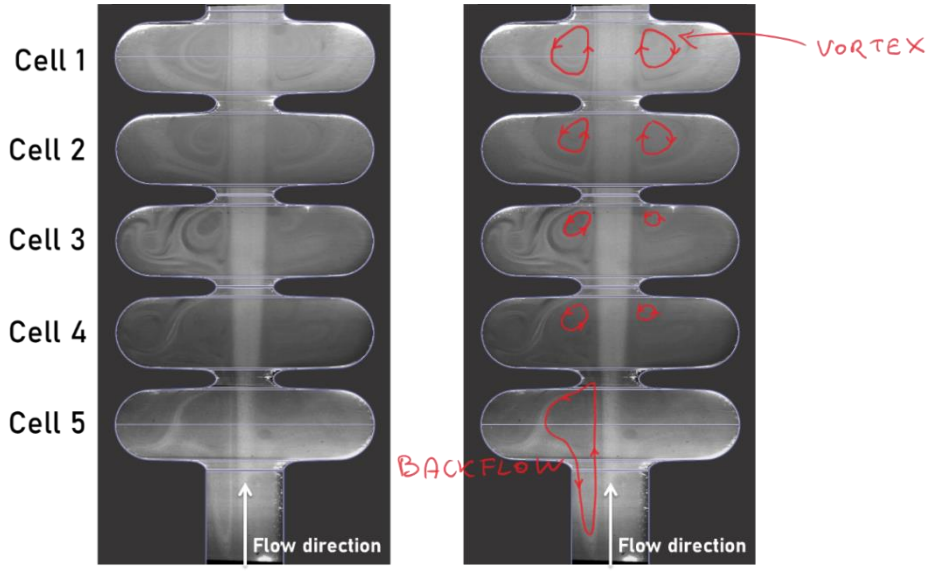

Figure 9. Stitched mean images visualizing the full flow field.

As the central flow impinges on the irises its outer region is pushed back and forced to recirculate generating two symmetrically located vortices, one to left and one to right of the central flow, see the red lines in cell 1, 2 and 3 of Figure 9. Those two vortices could be the section of a single toroidal vortex. Possibly, the backward flow originated by the impinging phenomenon is responsible for the vortices located in the radial outermost region of cells 4, 5, and 3, and visible in Figure 9.

Close to the inlet, i.e., at cells 5, the jet radius appears smaller than downstream, and a reverse flow

protruding upstream in the space between the central jet and the wall of the inlet duct clearly shows up, see the red line (backflow) shown in Figure 9. This recirculating flow could be due to the interaction between the central flow, the iris of the cell 5 and the blockage originated by the recirculating flow in cell 4.

3.2. PIV velocity maps

As already shown by the flow visualization, the mean flow field appears almost axial symmetric so only the left half of the velocity fields are described. Due to laser reflections at the walls and to a non-perfect image masking procedure some noisy vectors shows up in the velocity maps close to the walls. Figure 10(b) shows the mean velocity field at cells 1 and 2, as obtained from the original PIV images, i.e., with Δt =2.5 ms. The central flow shows velocities of about 2 orders of magnitude higher than those inside the cells, this can be related to the axial fluid injection and to the weak momentum exchange between those two regions. Using an interframe time of Δt =2.5 ms, the particle displacements in the low velocity region of the cells result to be much less than 0.1 pixels, thus the corresponding velocity vectors are quite noisy, Figure 10 (b). The accuracy of the low velocity vectors is significantly increased by applying the method described in section 2.3, compare Figure 10(a) and Figure 10(b).

Figure 10 clearly shows the vortices originated by the interaction between the central flow and the irises, and confirms the flow structure observed from flow visualizations, see section 3.1.

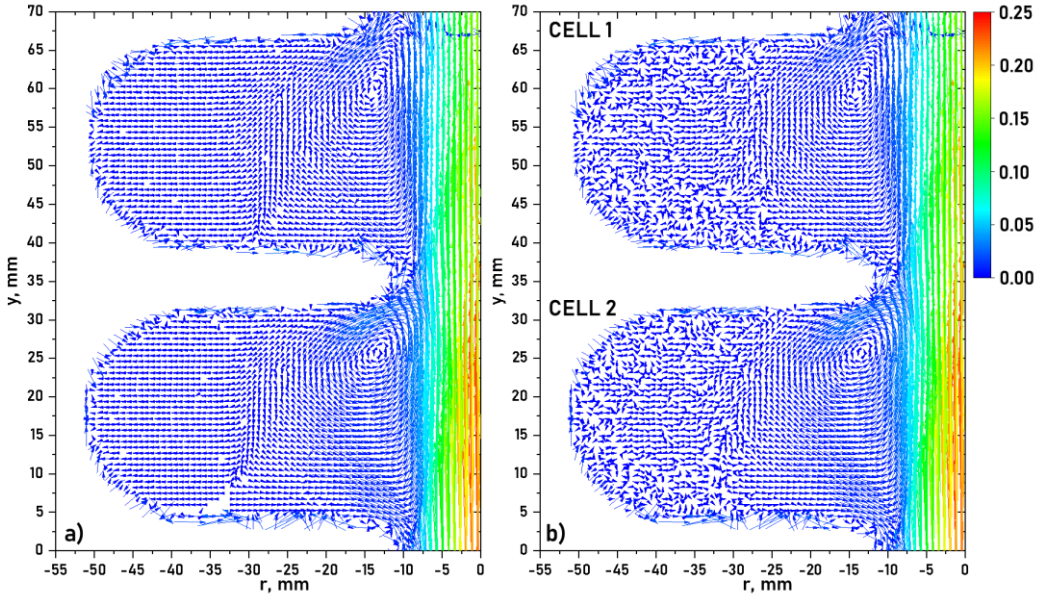

Figure 10. a) Hybrid mean velocity map (cells 1 and cell 2) reconstructed combining data from both Δt =2.5 ms and Δt =250 ms maps b) Mean velocity map (cells 1 and 2), Δt =2.5 ms. In colour is shown the magnitude of the velocity vector (m/s).

Figure 11 shows the mean velocity field at the inlet region, the latter comprises the cell 5 and the inlet duct. As already noticed some spurious vector shows up close to the cavity walls, moreover the possibly slightly misalignment of the laser sheet is not expected to significantly affect, at least qualitatively, the observed flow structure. The mean velocity map evidences a central fast flow directed upward, and a wide recirculating flow extending from the iris (located at about y= 67 mm) upstream down to y =0. At the iris, and close to the wall (x ≅8 mm and y ≅67 mm) it is visible a backflow coming from cell 4, this indicates a link between the flows in cells 5 and 4, but further investigations are needed to clarify this point.

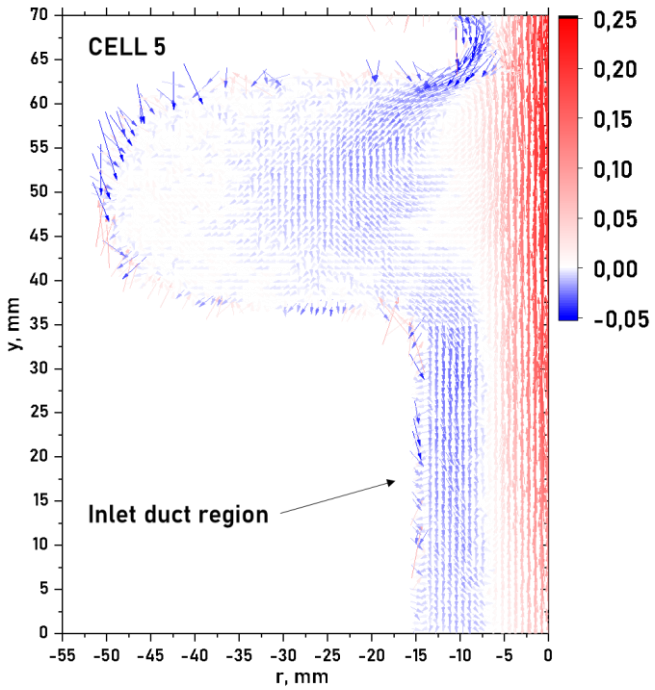

Figure 11. Mean velocity field in the inlet region. In color is shown the vertical velocity component (m/s), positive velocities are directed upward.

4. Conclusions and future developments

This paper reports a preliminary experimental work aiming at investigating the fluid dynamics of the BCP process by using the PIV and the refractive index matching (RIM) techniques, and to provide data for CFD validation. To the author's knowledge it is the first time that PIV and RIM techniques are applied to study such process.

The BCP process uses very toxic and dangerous acid mixtures, so a safer fluid (water+glycerol) and a downscaled transparent Sylgard 184 model of a SRF cavity are used. Both geometric and dynamic similarity are enforced, and the refractive index matching is achieved by using a mixture of about 61% and 39% in mass of glycerol and water, respectively. The experimental results collected so far evidence some interesting features of the model flow. A recirculating vortex is observed inside the cavity cells, and it is likely originated by the interaction between the central flow and the irises. Furthermore, a wide recirculating flow affects the whole inlet region (cell 5 and the inlet duct). The analysis of how these flow features depend on flow rate and acid injection could provide guidance on how to improve BCP treatment..

From the point of view of the experimental techniques, a very good RI matching is achieved by exploiting light deviation by a prism. Moreover, by pairing the first (or the second) frame of each couple of PIV images, it is possible to improve the accuracy of PIV measurements in the low velocity regions (i.e., the lobes of the SRF cavity), this is achieved at almost no costs. When the recoding frequency of the double images can be suitable adjusted, this approach allows to optimize the PIV measurements for both low and high velocities.

Our preliminary results demonstrated the capability of the PIV and RIM techniques to provide potentially useful data for understanding and improving the BCP treatment. Nevertheless, further PIV measurements and in-depth analysis are required to fully clarify the flow field structure and to provide data to validate CFD simulations.

Acknowledgements

The authors wish to thank FRALUMA for their commitment to a careful making of the phantom and of the aquarium, and particularly Mr. Collazuol Luca for his availability and for having suggested some solutions to improve the phantom design.

References

[1] Feder T 2010 Accelerator school travels university circuit *Phys. Today* **63** 20–2
[2] Holl M, Subramanian S and Xue Q 2001 Modeling and optimization of the chemical etching process in niobium cavities *Transactions of the American Nuclear Society* vol 85 (Hollywood, FL, United States: American Nuclear Society - ANS, La Grange Park (United States)) p 493
[3] Trabia M B, Culbreth W, Subramanian S and Tajima T 2004 Optimization of chemical etching process in niobium cavities *Proceedings of the ASME Design Engineering Technical Conference* pp 149–57
[4] Jones T and Pattalwar S 2017 Determining BCP Etch Rate and Uniformity in High Luminosity LHC Crab Cavities *18th International Conference on RF Superconductivity* (Lanzhou, China) pp 635–9
[5] Budwig R 1994 Refractive index matching methods for liquid flow investigations *Exp. Fluids* **17** 350–5
[6] Wright S F, Zadrazil I and Markides C N 2017 A review of solid–fluid selection options for optical-based measurements in single-phase liquid, two-phase liquid–liquid and multiphase solid–liquid flows *Exp. Fluids* **58**
[7] Amini N and Hassan Y A 2012 An investigation of matched index of refraction technique and its application in optical measurements of fluid flow *Exp. Fluids* **53** 2011–20
[8] Hopkins L M, Kelly J T, Wexler A S and Prasad A K 2000 Particle image velocimetry measurements in complex geometries *Exp. Fluids* **29** 91–5
[9] Cozzi F, Felisati G and Quadrio M 2017 Velocity measurements in nasal cavities by means of stereoscopic piv - preliminary tests *Journal of Physics: Conference Series* vol 882–012010
[10] Helmers T, Kemper P, Mießner U and Thöming J 2020 Refractive index matching (RIM) using double-binary liquid–liquid mixtures *Exp. Fluids* **61** 17
[11] Cheng N S 2008 Formula for the viscosity of a glycerol-water mixture *Ind. Eng. Chem. Res.* **47** 3285–8
[12] Prasad A K and Adrian R J 1993 Stereoscopic particle image velocimetry applied to liquid flows *Exp. Fluids* **15** 49–60
[13] Adrian R J and Westerweel J 2011 *Particle Image Velocimetry*